catalysts

MDPI

Article

Catalytic Oxidation of VOC over Cobalt-Loaded Hierarchical MFI Zeolite

Bozhidar Grahovski [1], Ralitsa Velinova [2], Pavletta Shestakova [3], Anton Naydenov [2], Hristo Kolev [1], Iliyana Yordanova [1], Georgi Ivanov [2], Krasimir Tenchev [1] and Silviya Todorova [1,*]

[1] Institute of Catalysis, Bulgarian Academy of Sciences, Acad. G. Bonchev St., Bldg. 11, 1113 Sofia, Bulgaria; rossonero_91@mail.bg (B.G.); hgkolev@ic.bas.bg (H.K.); ani4ka_pk87@abv.bg (I.Y.); tenchev@ic.bas.bg (K.T.)
[2] Institute of General and Inorganic Chemistry, Bulgarian Academy of Sciences, Acad. G. Bonchev St., Bldg. 11, 1113 Sofia, Bulgaria; raligeorgieva@svr.igic.bas.bg (R.V.); naydenov@svr.igic.bas.bg (A.N.); geoivanov@yahoo.com (G.I.)
[3] Institute of Organic Chemistry with Centre of Phytochemistry, Bulgarian Academy of Sciences, Acad. G. Bonchev St., bl. 9, 1113 Sofia, Bulgaria; Pavletta.Shestakova@orgchm.bas.bg
* Correspondence: todorova@ic.bas.bg; Tel.: +359-2-979-2576

Abstract: The zeolites ZSM-5 with different Si/Al ratios were modified with a buffer solution of HF and NH_4F. This acidic treatment led to the obtaining of a material with secondary mesoporosity. The deposition of cobalt from an aqueous solution of cobalt acetate on the surface of treated samples generates the formation of different cobalt oxide species: bulk-like Co_3O_4 phases strongly interacting with the support, Co^{2+} in ion exchange positions (γ and β sites) and silicate-like phases. The mechanism of cobalt silicate phase formation is proposed here and includes a replacement of silanol groups and the bridging hydrogens by Co and the inclusion of the Co atoms in tetrahedral framework positions. The catalysts, obtained through use of the treated ZSM-5, exhibit higher activity in the reactions of propane, and *n*-hexane completes oxidation compared with the catalyst samples containing un-treated zeolite. Both the finer dispersion of metal oxide particles on the hierarchical sample and the presence of secondary mesoporosity improve the effectiveness of the active phase utilization via access to larger number of active sites.

Keywords: hierarchical MFI zeolite; cobalt catalysts; catalytic combustion; propane; *n*-hexane

Citation: Grahovski, B.; Velinova, R.; Shestakova, P.; Naydenov, A.; Kolev, H.; Yordanova, I.; Ivanov, G.; Tenchev, K.; Todorova, S. Catalytic Oxidation of VOC over Cobalt-Loaded Hierarchical MFI Zeolite. *Catalysts* **2023**, *13*, 834. https://doi.org/10.3390/catal13050834

Academic Editors: Eduardo Miró, Ezequiel David Banus and Juan Pablo Bortolozzi

Received: 22 March 2023
Revised: 26 April 2023
Accepted: 27 April 2023
Published: 3 May 2023

1. Introduction

It is well known that the catalysts for CO oxidation and VOC combustion can be classified into three categories: (1) supported noble metals; (2) metal oxides or supported metal oxides; and (3) mixtures of noble metal and metal oxides. A major part of the commercial catalysts for these processes belongs to the first category, because the reaction can start at temperatures as low as room temperature. The high cost of precious metals, their limited availability and sensitivity to higher temperatures and poisons has motivated the search for substitute catalysts. Among all studied metal oxides, the most active single metal oxides are those of Cu, Co, Mn and Ni [1]. Manganese- and cobalt-containing catalysts are less expensive and demonstrate high activity in CO and VOCs oxidation [2,3].

The main drawback of the transition of metal oxides catalysts is the deactivation as result of an aggregation. This problem could be overcome by applying novel preparation methods and the application of supports with new properties, such as those of nanostructured porous oxides. Zeolites are such carriers, because of their specific pore structure, acidic properties, high thermal stability and their ability to exchange ions [4,5].

In recent years, the attention of scientists has focused on the use of zeolites as catalyst supports due to their thermal and acid stability and moisture resistance. They have a high specific surface area, which is a prerequisite for the creation of active catalytic systems. Metals and metal oxides can be deposited on them as highly dispersed nanoparticles and

thus create active catalytic systems in which a large number of active centers are accessible to the reagents in the catalytic processes. One of the best adsorbents and supports for catalytic systems used for the degradation of VOCs are zeolite aluminosilicates, thanks to their adjustable surface properties, their controllable hydrophobicity and their ability to deposit metals and metal oxides. The crystalline microporous structure characteristics of the zeolites, which imparts a high surface-to-volume ratio, is formed by tetrahedral units (TO_4) bonded by common oxygen atoms.

Zeolite ZSM-5 is a well-known high silicon crystalline aluminosilicate with wide areas of applications as a catalyst and sorbent. Its chemical formula is $|Na^{+}{}_n(H_2O)_{16}|[Al_nSi_{96-n}O_{192}]$, where n < 27, and its structure is made up of five membered rings, forming the composite building units "mfi", "mor", "cas" and "mel". By combining the building units a structure is formed, containing intersecting channel systems. Ten-member straight channels (0.53 × 0.56 nm) are located i the crystallographic direction [010], while ten-member twisted channels (0.51 × 0.55 nm) [6–8] are contained in the [100] direction. Although it belongs to the group of medium porous zeolites, ZSM-5 has a relatively high resistance to coke formation. Due to the combination of high hydrothermal structural stability and large surface area to volume ratio, this zeolite is widely used in reactions that rely on chemical and physical interactions occurring on the crystalline surface [9,10]. One of the disadvantages of zeolites as a catalyst for oxidation reactions is the deposition of coke on the surface, which leads to deactivation [11]. One way to overcome this drawback is the development of tailored hierarchical zeolites, which have been proven to significantly increase catalysts' tolerance to coking [12]. One approach for obtaining secondary porosity is through treatment with a buffer solution of hydrofluoric acid and ammonium. The method was first reported by V. Valtchev et al. [13]. Whereas F^{-} selectively etches aluminum from the crystal structure, the HF^{2-} formed in the buffered solution exhibits a slightly higher reactivity and non-selectively extracts both framework elements (silicon and aluminum) [13,14].

In our previous articles, the propane and *n*-hexane oxidation in the presence of cobalt-modified zeolite ZSM-5 with different Si/Al ratio were studied [15,16]. It was found that the high catalytic activity of Co–ZSM-5 (Si/Al = 23) in both reactions was the result of the high reducibility due to the lower interaction of the cobalt oxide with the support. Based on the study of the reaction kinetics, the Mars–van Krevelen mechanism was considered to be the most probable for propane oxidation and the Langmuir–Hinshelwood model was used for complete n-hexane oxidation.

In this study, the results concerning the complete oxidation of VOCs in the presence of cobalt catalysts supported on hierarchical zeolite ZSM-5 with different Si/Al are described. The additional porosity was introduced via acid treatments with HF acid in combination with NH_4F buffer. Our expectation was that obtaining a second level of porosity would increase the catalytic activity as a result of the improved access of reactants to the active sites. A similar effect was observed in hierarchical MFI zeolites modified with Pt and Cu in CO and benzene complete oxidation [17], as well as hierarchical mordenite in the reaction of m-xylene transformation [18].

2. Results

2.1. X-ray Diffraction

Figure 1a depicts the X-ray diffraction patterns of the zeolite ZSM-5 (par) with different Si/Al and the materials treated with an aqueous solution of 0.25 M HF, and NH_4F denotes ZSM-5 (tr). According to the literature data the strong diffraction peaks appear at in the ranges of 2θ = 7°–9° and 2θ = 23°–25° in all the XRD patterns, corresponding to the standard patterns of ZSM-5 zeolite [19]. The crystallinity and structural characteristics were preserved in the acidic treatment samples. The X-ray patterns of cobalt-modified samples are shown in Figure 1b.

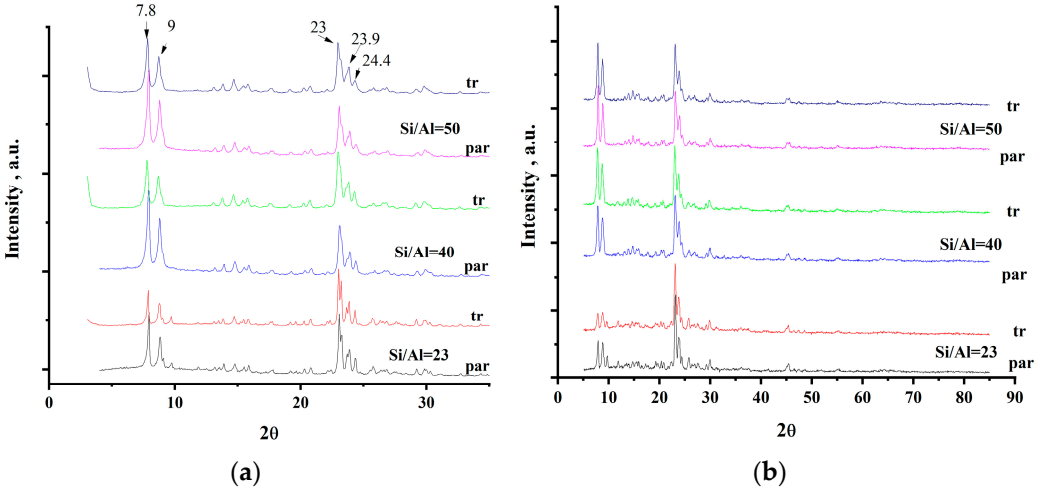

Figure 1. XRD patterns of (**a**) parent and treated ZSM-5 samples; (**b**) parent and treated samples impregnated with cobalt.

No diffraction lines for Co_3O_4 or cobalt silicates are observed in the case of the cobalt supported by the treated ZSM-5 samples. The presence of a Co_3O_4 phase was confirmed using the TPR data and the UV-VIS results. The absence of diffraction lines for Co_3O_4 is the confirmation for high dispersion of this phase in the treated samples. The formation of cobalt silicate in treated zeolites is confirmed by the blue color of all samples. In previous studies [15], it was found that the cobalt in Co-ZSM-5 (Si/Al = 23) catalyst mainly represents a well crystallized Co_3O_4 phase and that a major part of cobalt in the Co-ZSM-5 (Si/Al = 40) sample is in the form of finely dispersed Co_3O_4. Obviously, the acid treatment of zeolites promotes the formation of finely dispersed Co_3O_4 on the catalyst's surface and silicate-like surface phases.

2.2. Nitrogen Physisorption

The specific surface areas and micro-/mesopore volumes of parent and treated ZSM-5 were analyzed via physical nitrogen adsorption (Table 1 and Figure 2). As was discussed in our previous investigation concerning the parent ZSM-5 zeolites [16], type IV isotherms with a hysteresis loop from $P/P_0 = 0.45$ to $P/P_0 = 1$, which were caused by the coherence of both micropores and mesopores (Figure 2), were obtained. The higher nitrogen uptake was observed in the isotherms of the samples after acid attack (Figure 2) at partial pressure close to 1 as a result of the secondary porosity and reduced crystallite size [17]. This is more pronounced in the sample with Si/Al = 50.

Table 1. Textural properties and elemental analysis of parent and treated ZSM-5 zeolites.

Samples	S_{BET}, (m^2/g)	V_t [a] (cm^3/g)	Average Pore Diameter (nm)	V_{micro} [b], (cm^3/g)	V_{sec} [c] (cm^3/g)	Si/Al [d] (mol/mol)
Si/Al = 40 par	331	0.25	3.0	0.16	0.09	34.2
Si/Al = 23 par	349	0.20	2.3	0.16	0.04	22.2
Si/Al = 50 par	340	0.25	3.4	0.15	0.10	47.8
Si/Al = 40 tr	392	0.30	3.4	0.15	0.15	37.5
Si/Al = 23 tr	358	0.25	3.3	0.15	0.15	39,6
Si/Al = 50 tr	442	0.60	6.5	0.15	0.45	47.8

[a] V_t—total pore volume; [b] V_{micro}—microporous volume evaluated using the Vt method; [c] V_{sec}—secondary meso- and macropores formed through chemical treatment ($V_{sec} = V_t - V_{mi}$), [d] according to XRF (X-ray fluorescence) analysis.

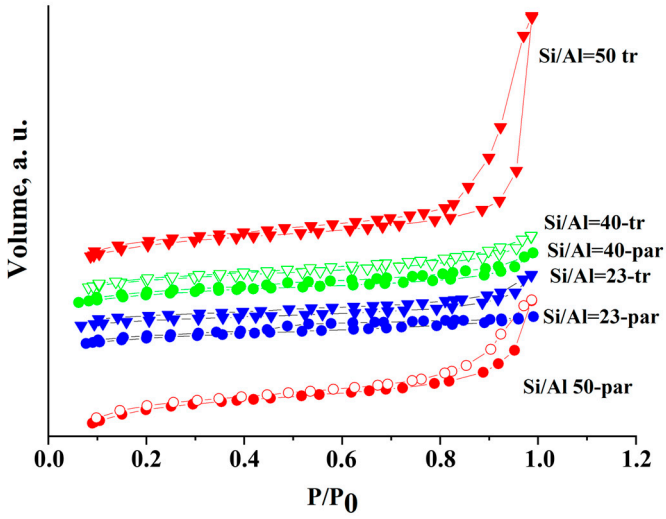

Figure 2. Nitrogen adsorption/desorption isotherms of parent and treated ZSM-5 with different ratios of Si/Al.

After the acidic treatment, the changes in textural properties (specific surface area and pore volume) for all zeolites were observed. The increase in specific surface, decrease in micropore volume and increase in the volume of the mesopores was observed. It can be seen that samples subjected to acidic treatment increased the volume of the secondary mesopores, which is most pronounced in sample Si/Al = 50, where it increases more than fourfold. Elemental analysis shows the slight increases in the Si/Al ratio of samples Si/Al = 23 and Si/Al = 40 in comparison with that of the parent zeolite. These results mean a weak process of dealumination and no change in the Si/Al ratio for a sample of Si/Al= 50. These results indicate that a relatively similar amount of both elements (Si and Al) were extracted from the zeolite structure.

2.3. X-ray Photoelectron Spectroscopy

The oxidation states of Co on the surface were examined using XPS. Figure 3 shows an example curve fitting of $Co2p_{1/2}$ before and after the reaction.

The surface atomic concentrations of cobalt and the peak position of samples before and after the reaction are presented in Table 2. A peak within the energy range of 792–798 eV was measured for cobalt with defined binding energies (BEs) either of 795.2–796 eV (Co^{3+}) or 797.1–798 eV (Co^{2+}), respectively [20,21]. The presence of Co^{2+} ions in the cobalt-containing samples is confirmed by the presence of a peak with a binding energy of 797.8 eV. As is visible from Table 2, the Co^{2+} is the only species on the surface of the sample before the reaction with Si/Al = 50-tr and Si/Al = 40-tr, and it was dominant on the surface of Si/Al = 23-tr catalyst before the reaction. It was shown in our previous investigation that the Co^{3+} is the dominant species on the surface of non-treated Co-ZSM-5with Si/Al = 23 before and after the reaction [15] and part of the cobalt in sample with Si/Al = 40 presents as Co^{3+}. Obviously, the acidic treatment of the zeolites favors the formation of surface Co^{2+} ions. Another feature that can be seen from the Table 2 is that the surface cobalt concentration changes very little after reaction, which could be explained by the stabilization of the different cobalt species in the zeolite framework.

For the samples Co-ZSM-5 Si/Al = 23 and Si/Al = 40, the Co^{2+} part was oxidized to Co^{3+} after the reaction, leading to the increase in its concentration.

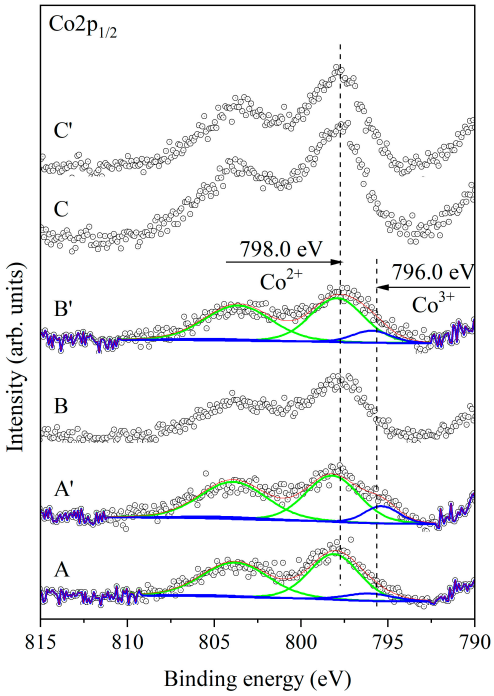

Figure 3. Fitted Co2p1/2 photoelectron peaks of Co-ZSM-5-tr catalysts with different Si/Al ratios: Sample A—Si/Al = 23; B—Si/Al = 40; C—Si/Al = 50—before catalysis; A′—Si/Al = 23; B′—Si/Al = 40; and C′—Si/Al = 50—after *n*-hexane oxidation.

Table 2. Surface atomic concentrations of cobalt in the Co-ZSM-5 catalysts.

	Co2p$_{1/2}$		
Before Catalysis			
	Si/Al = 23-A		
Conc., at.%		1.96 *(par-2.61)* *	
BE, eV	796.1		798.1
Conc., at.%	0.17 *(2.11)*		1.79 *(0.5)*
	Si/Al = 40-B		
Conc., at.%		1.93 *(par-2.26)*	
BE, eV			797.9
Conc., at.%	*(0.04)*		*(2.22)*
	Si/Al = 50-C		
Conc., at.%		3.64 *(par-4.76)*	
BE, eV			798.0
Conce, at.%			
After catalysis			
	Si/Al = 23-A′		
Conc., at.%		2.11	
BE, eV	795.4		798.2
Conc., at.%	0.31		1.80
	Si/Al = 40-B′		
Conc., at.%		1.86	
BE, eV	795.9		797.9
Conc., at.%	0.24		1.62
	Si/Al = 50-C′		
Conc., at.%		3.41	
BE, eV			797.8
Conc., at.%			3.41

* The data for the starting zeolite, according to [15], are presented in brackets in italics.

2.4. Temperature-Programmed Reduction by Hydrogen

The TPR profiles of a cobalt-modified parent and the treated catalyst samples are shown in Figure 4. Their patterns can be deconvoluted up to 450 °C into three main constituents with low-temperature shoulders, at 290 °C for Si/Al = 23 and 310 °C for Si/Al = 40, with the sharpest and most well-distinguished peak located in the range 324–342 °C, and the broad peak was found at about 380 °C.

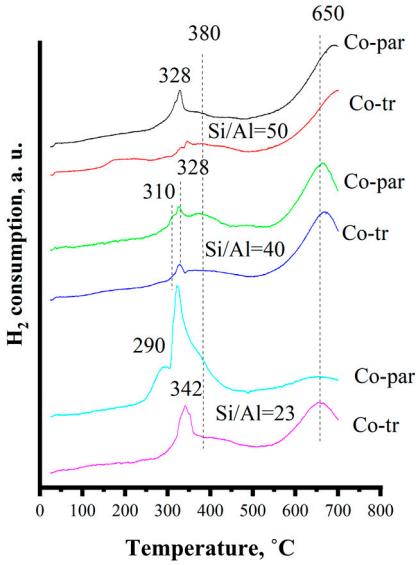

Figure 4. H_2-TPR spectra of parent and treated Co-ZSM-5 catalysts having different Si/Al ratios (23, 40 and 50) (gas mixture of 10% H_2/N_2, 10 mL min^{-1}).

The first two reduction peaks fit well in the reduction interval observed previously in bulk Co_3O_4 powder or large supported Co_3O_4 particles [22]. The peak at 290(310) °C is attributed to the reduction of Co_3O_4 to CoO and the next higher temperature originates from the reduction of CoO to Co^0. The shoulder, which is centered at 380 °C, is ascribed to small particles that strongly interact with the support [23]. As can be seen from the TPR profiles, the reduction temperatures of the treated samples are shifted to higher values, while at the same time the parts of surface species that are reduced at temperatures above 650 °C also increase. It was shown in our previous investigation that the peaks of Co-ZSM-5-par with Si/Al = 23 appear at lower temperatures in comparison with those of the other samples [15] and that the formed oxide particles are the largest in the series and as a consequence they are reduced at the lowest temperature [24–26]. All treated samples manifested an increase in hydrogen consumption above 600 °C. According to the literature data, the hydrogen consumption above 600 °C is due to the reduction of mono-atomic Co^{2+} or $CoOH^+$ ions at the exchange sites [27–30]. The main ion present in the cobalt acetate solution exchange of the parent H-ZSM-5 is $[Co\text{-}OH]^+$, which suggests that Co^{2+} cation replaces one zeolitic proton to lead to a monomeric species $[Co\text{-}OH]^+$ [15,31]. The following can be summarized from the TPR studies: a slight shift in the reduction maxima for Co_3O_4 at higher temperatures increases the hydrogen consumption in the region of the reduction of Co_3O_4 particles, which strongly interact with the support, and in the region in which Co^{2+} species are reduced. All these changes demonstrate stronger interactions between the cobalt oxide phases and the zeolite framework in the case of treated samples. The additional formation of different Co^{2+} species is also the reason for the increased Co^{2+} surface concentration established from the XPS data (Table 2) for Si/Al = 23 sample after the reaction.

2.5. UV-Vis Spectroscopy

UV-vis spectra provide additional information about cobalt species present in the Co-ZSM-5 catalyst (Figure 5). The bands at 412 nm, 498 nm, 521 nm, 594 nm, 650 nm and

770 nm are visible on the UV-vis spectra of treated samples. According to the literature data, these bands are ascribed as follows: 498 nm o Co^{2+} ions in the sinusoidal channel of ZSM-5 (γ sites) [32,33] and 521 nm, 594 nm and 638 nm to Co^{2+} ions located at the intersection of the straight and sinusoidal channels (β site) [28,32,33] and 750 nm external Co_3O_4 oxide [28]. The presence of Co_3O_4 in all the studied samples is evidenced by the appearance of peaks at 412 nm and 770 nm (see Table 3 and Figure 4).

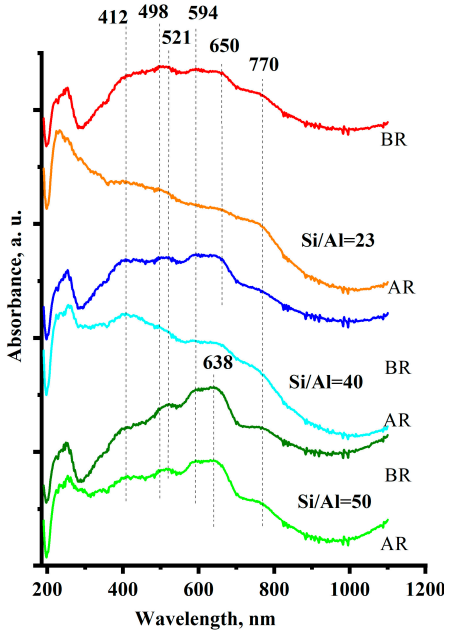

Figure 5. UV–vis spectra of treated Co-ZSM-5 catalysts with different Si/Al ratios (23, 40 and 50) before (BR) and after *n*-hexane oxidation (AR).

Table 3. Assignment of UV–vis peaks for various Co species.

Wavelength, nm	Assignment	References
500	Co^{2+} in octahedral symmetry as either $[Co(H_2O)_6]^{2+}$ or $[Co(H_2O)_5OH]$	[34]
498	Co^{2+} ions in the sinusoidal channel of ZSM-5 (γ sites)	[32,33]
521, 594 and 638	Co^{2+} ions located at the intersection of the straight and sinusoidal channels (β site)	[29,32,33]
662	Co^{2+} ions coordinated to the rectangle of four O atoms of the walls of the main ZSM-5 channels (α site)	[32,33]
417 and 750	external Co_3O_4 oxide, octahedrally coordinated Co^{3+} in the mixed spinel oxide phase Co_3O_4	[28,35]

According to our previous studies concerning cobalt deposited on a parent SZM-5 zeolite with a ratio of Si/Al = 23, only the bands for Co_3O_4 were found. After the acid treatment of this sample, bands for Co^{2+} ions in different positions are also visible. Obviously, the acidic treatment with HF and NH_4F of the parent zeolite with a ratio of Si/Al = 23, favors the access of $[Co\text{-}OH]^+$ ions during impregnation into the pores of the zeolite and their location in the intersection of the straight and sinusoidal channels. In case of cobalt-modified parent zeolite with a ratio of Si/Al = 40, in addition to the bands for Co_3O_4 and the bands for Co^{2+} ions at the γ sites (sinusoidal channel of ZSM-5), the presence of Co^{2+} ions at the β site were observed [15]. The band for Co^{2+} ions at the α sites (662 nm) is not visible. The all data from UV-vis are in accordance with the TPR study where it was shown that the presence of the reduction maxima corresponded to the reduction in Co^{2+} ions in the exchanged position. Based on the spectra after reaction, it

can be assumed that there is no significant change in the type and location of the different cobalt species.

2.6. SEM

The SEM micrographs of initial and treated ZSM-5 zeolite with an Si/Al-23 ratio are shown in Figure 6. Figure 6a corresponds to the parent ZSM-5 zeolite and 6b and 6c to the treated ZSM-5, respectively. In ZSM-5 (Si/Al = 23), the formation of aggregates of sizes of about 2–3 μm was observed, while after the acid attack, the crystal size was decreased about two times, very likely as a result of the destruction of the primary crystals [18]. The SEM image with higher magnification shows the particles as having a rough surface and a mesoporous formation.

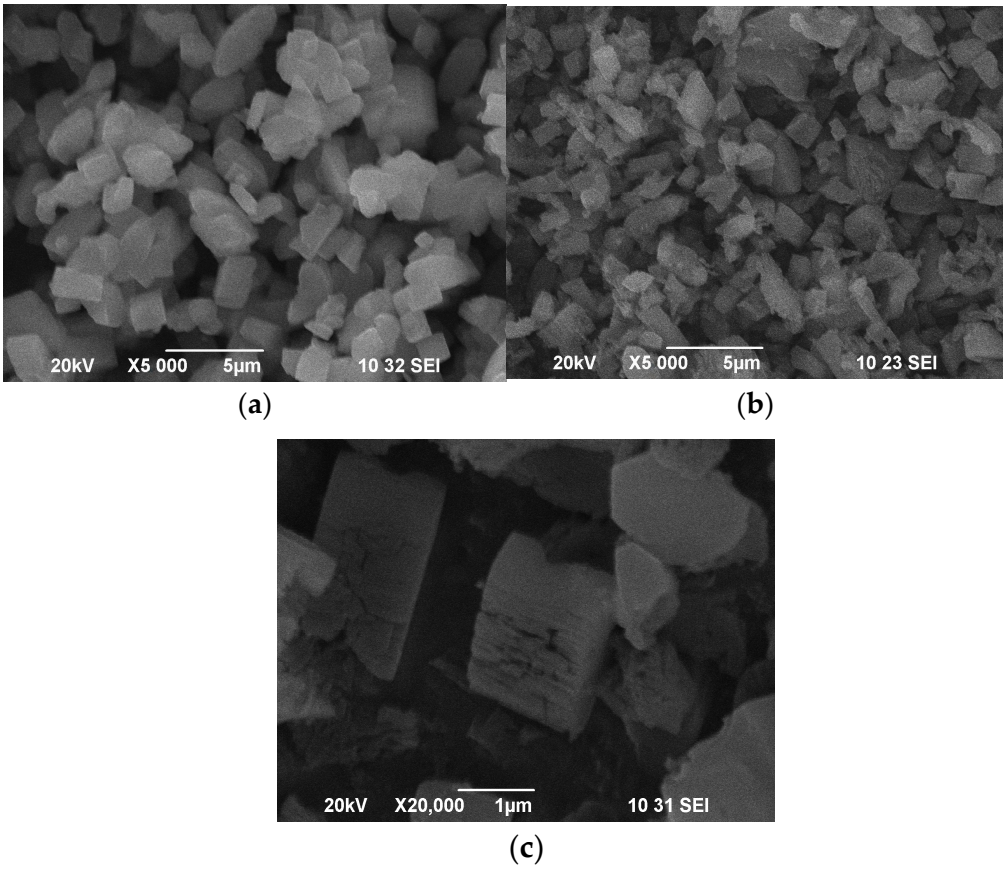

Figure 6. SEM micrographs of (**a**) the ZSM-5 Si/Al = 23 parent sample and (**b**,**c**) samples obtained via treatment with an HF-NH_4F mixed solution.

The SEM micrographs of untreated and treated ZSM-5 with Si/Al = 50 are presented in Figure 7. As can be seen this sample is made up of a large number of particles (about 0.5 μm) with a rough surface (Figure 7a). After acidic treatment the particle size decreases (Figure 7b). It was established that the zeolite dissolution through HF initially affects the structural defects and/or the adhesion positions of the individual crystallites and then continues deep inside the crystals [17]. As can be seen from the SEM micrograph that the Si/Al = 50 sample has the smallest aggregates among all studied samples. Therefore, the presence of more structural defects in this sample could be assumed, facilitating the dissolution of the zeolite and the formation of mesopores.

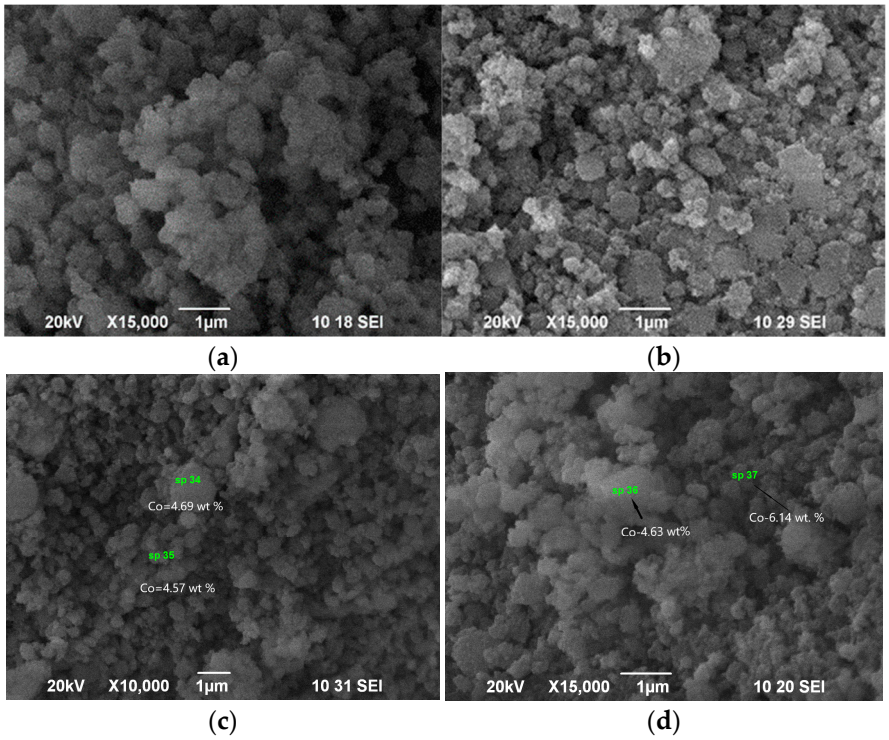

Figure 7. The SEM micrographs of (**a**) untreated and (**b**) treated ZSM-5 Si/Al = 50; (**c**,**d**) EDX of different areas.

The EDX analysis of different regions of the Co-ZSM-5-tr (Si/Al = 50) sample indicated the homogeneous distribution of Co on the support.

2.7. NMR Analysis

The most active sample Co-modified acid-treated (Co-ZSM-5-tr), parent ZSM-5 (Si/Al = 50) and the acid-treated (ZSM-5-tr) zeolites were investigated using solid state NMR spectroscopy to obtain a more detailed insight into the structural characteristics of the studied materials at the atomic level.

The ^{29}Si NMR spectra with direct excitation (single pulse spectra) allowed the quantitative assessment of the composition of the zeolite framework and the determination of the Si/Al ratio by using the relative areas of the characteristic resonances of the different Si(nAl) units (n = 0,1,2,3,4): Si(4Al), Si(3Al), Si(2Al), Si(1Al) and Si(0Al) [36]. Figure 8 presents the ^{29}Si single pulse spectra of the parent, the acid-treated ZSM-5 and the Co-modified ZSM-5-tr samples.

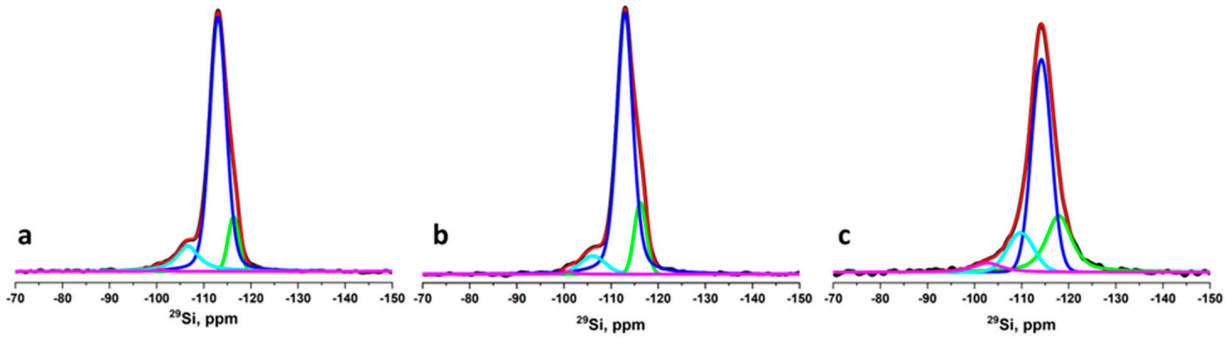

Figure 8. Experimental (black) and simulated (red) single-pulse ^{29}Si NMR spectra of the studied zeolites: (**a**) parent ZSM-5, (**b**) acid-treated ZSM-5 (ZSM-5-tr) and (**c**) Co-modified Co-ZSM-5-tr. The individual contributions of the different Si environments are shown as colored lines (green, blue, cyan, magenta).

The results from the deconvolution of the spectra using DMFit software [37] are summarized in Table 4.

Table 4. NMR parameters obtained through the deconvolution of the ^{29}Si single pulse NMR spectra.

Sample	Si(0Al)		Si(0Al)		Si(1Al)		Si(2Al)/Si(1OH)		Si/Al Ratio
	ppm	%	ppm	%	ppm	%	ppm	%	
ZSM-5(Si/Al = 50)	−116	10	−113	76.5	−107	13	−101	0.5	31
ZSM-5-tr(Si/Al = 50)	−116	13	−113	78	−106	8	−101	1	40
Co-ZSM-5-tr(Si/Al = 50)	−118	21	−114	60	−109	17	−103	2	19

The spectra of the parent ZSM-5 and acid-treated ZSM-5-tr samples display the typical pattern for ZSM-5 zeolites with three main resonances: the signals at −116 ppm and −113 ppm are assigned to two tetrahedral Si(0Al) sites, which are crystallografically non-equivalent, while the signal at −107 ppm is characteristic for Si(1Al) structural units [38–41]. An additional low intensity peak at around −102 ppm is also identified after the deconvolution of the spectra. This peak indicates the presence of a small amount of Si(2Al) and/or Si(1OH) structures. Silanol groups from framework defects, for example, $Si(OH)(OSi)_{3-n}(OAl)_n$, exhibit peaks, shifted to the low field from the corresponding Si(nAl) species and, therefore, may partially overlap with the resonances of the Si[(n + 1)Al] units. The results presented in Table 4 demonstrate that sample treatment resulted in changes in Si/Al ratio determined by NMR (the last column in Table 4). For the acid-treated ZSM-5-tr sample an increase in the Si/Al ratio was observed, indicating the possible dealumination of the zeolite framework. The overall spectral characteristics of the parent and acid-treated materials are quite similar, indicating that acidic treatment is not associated with significant changes in the zeolite structure. The ^{29}Si spectrum of the Co-modified sample Co-ZSM-5-tr, however, shows some differences in its spectral pattern. All resonances in the spectrum of the Co-modified sample are shifted to a higher field and the calculated Si/Al ratio is significantly lower. The Si/Al ratio calculated from the EDX analysis of the parent, the treated and the Co-modified sample with Si/Al = 50 are 46, 44 and 42 s respectively. The differences in the Al/Si ratios obtained using the different methods are probably due to the different accuracies of the determination. What is clearly seen is that the deposition of cobalt from cobalt acetate leads to a decrease in the Al/Si ratio. The decrease in the Si/Al ratio in Co-modified samples indicates that the introduction of Co is associated with compositional and structural transformations of the zeolite framework. We suggest that the Co-modification resulted in the simultaneous removal of Si and Al atoms from the zeolite framework and inclusion of the Co atoms in tetrahedral framework positions. A similar phenomenon has been suggested by Mhamdi et al. [42] for the formation of cobalt silicate when cobalt is deposited from acetate onto ZSM-5. The authors suggest that the fragile H-ZSM5 appears to be unstable toward acetic acid produced during heating through a reaction between H+ and acetates, from the decomposition of the cobalt salt. The consequences are a superficial destruction of the zeolite grains and a local dealumination leading to a phase rich in silicon that accommodates the cobalt ions in tetrahedral symmetry (hence the blue color of the powder) and to extra framework aluminum atoms. The evidence of the tetrahedral coordination of cobalt in our sample is its blue color after calcination. In addition to this, the Co^{2+} cations can play the role as charge-compensating ions through the substitution of the bridging hydrogen ions. In the next step, we used $^{1}H \rightarrow ^{29}Si$ cross polarization (CP) MAS NMR spectroscopy with the aim to identify the presence of SiOH groups that are often generated as defect sites in the zeolite framework during synthesis and modification procedures. The CP technique is based on the transfer of magnetization from abundant spins (^{1}H) to low sensitivity nuclei (^{29}Si) via space dipole–dipolar interactions, resulting in a selective enhancement of the resonances from ^{29}Si units with ^{1}H in their vicinity, such as Si-OH groups or Si(nAl) sites with adjacent H atoms. The overlayed $^{1}H \rightarrow ^{29}Si$ CP MAS spectra and ^{29}Si single pulse spectra of the parent ZSM-5 and the acid-treated ZSM-5-tr are presented in Figure 9.

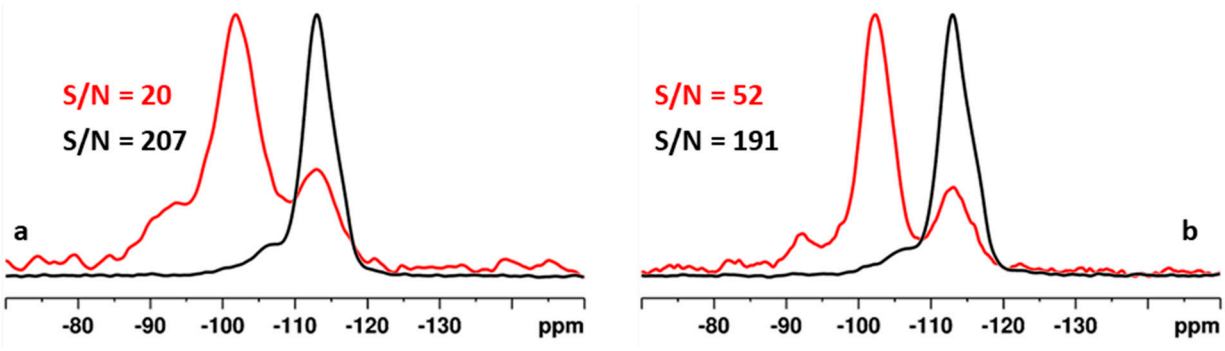

Figure 9. Comparison of the $^{1}H \rightarrow ^{29}Si$ CP (red) and single-pulse (black) ^{29}Si NMR spectra of the studied zeolites: (**a**) parent ZSM-5 and (**b**) acid-treated ZSM-5 (ZSM-5-tr).

The $^{1}H \rightarrow ^{29}Si$ CP spectra of the two samples display three main resonances. The most enhanced resonance at −102 ppm is characteristic for Si(1OH) groups, while the low intensity signal at −92 ppm indicates the presence of a small amount of Si(2OH) units. The main resonance observed in the ^{29}Si spectra at −113 for the Si(0Al) sites is also slightly enhanced due to possible transfer of magnetization from neighboring silanol protons, charge compensating protons and/or coordinated water molecules. Since the resonance at −102 ppm for the Si(1OH) partially overlaps with the signal of Si(2Al) species, the actual Si/Al ratio might be slightly underestimated. The effectiveness of magnetization transfer in the $^{1}H \rightarrow ^{29}Si$ CP MAS technique, and thus the magnitude of enhancement, depends on many factors, such as Si—H internuclear distances, the relaxation rates and local dynamics of the structural fragments, which vary from one chemical environment to another. Therefore, the $^{1}H \rightarrow ^{29}Si$ CP MAS spectra are not applicable for quantitative assessments. Nevertheless, we can safely assume that there are a relatively small number of silanol groups, since CP efficiency was very low and a high number of scans (NS > 20,000) were necessary to achieve a reasonable signal-to-noise ratio (S/N) in the $^{1}H \rightarrow ^{29}Si$ CP spectra of both the parent (S/N = 20) and the acid-treated sample (S/N = 52). For comparison in the quantitative single pulse experiments, a much higher S/N of 207 for the ZSM-5 and 191 for the acid-treated ZSM-5-tr zeolites was achieved with 1024 scans (Figure NMR2). The S/N ratio detected in the $^{1}H \rightarrow ^{29}Si$ CP spectrum of the parent ZSM-5 was lower by a factor of 2.6 as compared to the S/N ratio in the spectrum of the ZSM-5-tr, obtained under identical experimental conditions (NS, relaxation delay, mixing time, etc.). We were not able to successfully record a $^{1}H \rightarrow ^{29}Si$ CP spectrum of the Co-modified Co-ZSM-5-tr sample, and even across 20,000 scans and several different mixing times, the CP efficiency was very bad, resulting in very noisy spectra. The low efficiency can be explained by the possible replacement of the silanol groups and the bridging hydrogens by Co, thus limiting the main source of magnetization transfer. On the other hand, the cobalt is a quadrupolar (I = 7/2) nucleus, and Co^{2+} in particular is paramagnetic and can therefore induce the rapid relaxation of the neighboring protons, which also results in a very low CP efficiency.

The ^{27}Al NMR is an important method for the investigation of the Al coordination state, the local symmetry of the Al structural environment and the nature of the Al species in the zeolite framework. The ^{27}Al NMR spectra of the parent, acid-treated and Co-modified ZSM-5 zeolites (Figure 10) are dominated by the signals of the tetrahedrally coordinated framework Al atoms centered at around 57 ppm.

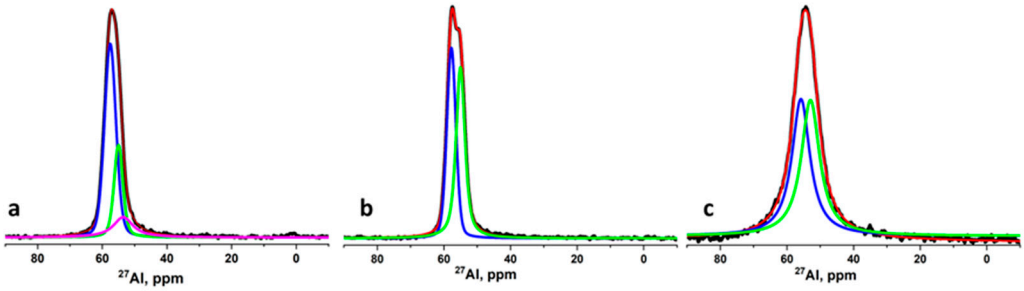

Figure 10. Experimental (black) and simulated (red) single-pulse 27Al NMR spectra of the studied zeolites: (**a**) parent ZSM-5, (**b**) acid-treated ZSM-5 (ZSM-5-tr) and (**c**) Co-modified Co-ZSM-5-tr. The individual contributions of the different Al environments are illustrated as colored lines (green, blue).

The presence of six coordinated extra-framework Al species (EFAl) with a characteristic resonance at around 0 ppm has not been detected. The results from the deconvolution of the spectral patterns with DMFit software are summarized in Table 5. The data for the parent ZSM-5 indicate the presence of three resonances originating from different types of the tetrahedrally coordinated Al atoms. The two relatively narrow resonances at 58 and 55 ppm are characteristic for two types of framework Al structures with slightly different symmetry of their environment. The broad third resonance at ~53 ppm is assigned to distorted tetrahedrally coordinated Al species at the defect positions of the zeolite framework [40–44].

Table 5. NMR parameters obtained via the deconvolution of the ^{27}Al NMR spectra.

Sample	Al1			Al2			Al3		
	ppm	%	$\nu_{1/2}$ (Hz)	ppm	%	$\nu_{1/2}$ (Hz)	ppm	%	$\nu_{1/2}$ (Hz)
ZSM-5(Si/Al = 50)	58	61	625	55	25	516	53	14	1141
ZSM-5-tr	58	49	500	55	51	500	-	-	-
Co-ZSM-5-tr	-	-	-	56	42	1047	53	58	1141

In the ^{27}Al spectrum of the acid-treated ZSM-5-tr, the two main signals have a narrower linewidth, while the broad resonance was not detected. These observations imply that the Al sites in the ZSM-5-tr zeolite have higher symmetry and the acidic treatment therefore resulted in a higher degree of ordering and a better structuring of the zeolite framework. The ^{27}Al spectrum of the Co-modified zeolite shows a broad spectral pattern that could presumably be deconvoluted to two broad signals centered at 55 ppm and 53 ppm. The substantial broadening of the ^{27}Al resonances could be explained by the significant deformation of the ^{27}Al structural environment, resulting from the inclusion of the Co atom in framework positions. The presence of surface Co^{2+} ions, which are paramagnetic, also contributes to line-broadening effects.

2.8. Catalytic Activity Test

All prepared samples were investigated for their catalytic activity behavior in the total oxidation reaction of propane and *n*-hexane. The results for the Co-ZSM-5 catalysts with different ratios (Si/Al = 50, Si/Al = 40 and Si/Al = 23) are shown in Figure 11.

As can be seen from Figure 11, the catalytic activity increased in the acid-treated samples, and this was most visible for the sample with a ratio of Si/Al = 50. In the case of propane oxidation, no change in the activity of the Co–ZSM-5 catalyst with a ratio of Si/Al = 40 was observed. The most remarkable aspect is the increase in catalytic activity in the complete *n*-hexane oxidation reaction. In this case, an increase in activity as observed for all three treated samples, the weakest being the sample with a ratio of Si/Al = 23, followed by the sample with a ratio of Si/Al = 40 and the sample with highest activity was that with a ratio of Si/Al = 50.

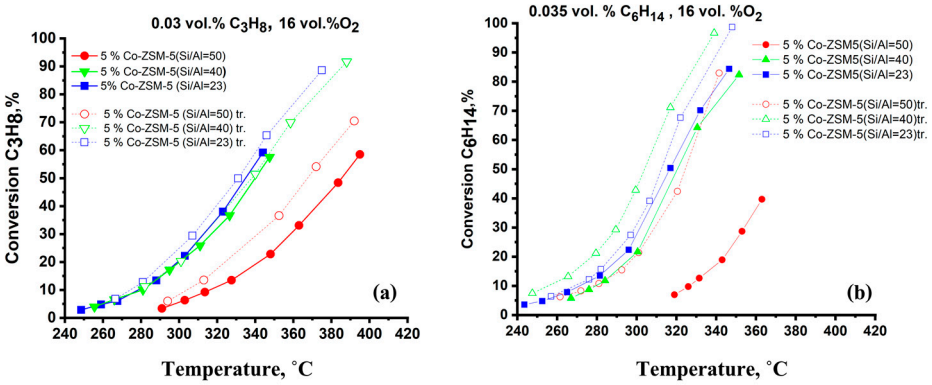

Figure 11. Temperature dependence of (**a**) propane oxidation and (**b**) *n*-hexane complete oxidation on parent and treated Co-ZSM-5 catalysts with different Si/Al ratios (23, 40 and 50).

In our previous investigation, it was found that the Co–ZSM-5 (Si/Al = 23) catalyst manifested the highest catalytic activity in the complete oxidation reactions of propane and *n*-hexane as a result of the high reducibility and the lower interaction of the cobalt oxide with the support [15,16]. Based on the study of the reaction kinetics, the Mars–van Krevelen mechanism was the most probable for propane oxidation and the Langmuir–Hinshelwood mechanism was the most likely for complete *n*-hexane oxidation.

It is well known that when the catalysts operate in the oxidation reactions through a Mars–van Krevelen mechanism the VOCs are oxidized via the solid, and the catalytic activity is directly correlated with the catalyst reducibility. Oxides that are reduced at a lower temperature exhibit higher catalytic activity. As mentioned above, the cobalt oxide phases in the treated samples are reduced at higher temperature. In such a case, it cannot be supposed that the reduction behavior determines the catalytic activity. Obviously, the improved access to the active sites in the treated samples plays an essential role.

A similar result has been observed in platinum, copper and palladium catalysts supported on hierarchical MFI zeolite in the oxidation reactions of CO and benzene [17]. A more noticeable effect of acid treatment on the activity of the complete *n*-hexane oxidation is most likely related to the fact that the *n*-hexane molecule ($d_{n\mathrm{Hex}}$ = 10.3 Å) [45] is larger than that of propane and the presence of secondary mesoporosity had a higher effect on *n*-hexane oxidation.

For the reliable and quantitative analysis of the catalytic activity of the samples and the effect of the treatment, the ratio between the pre-exponential factors at apparent fixed averaged activation energies, $k_{o,tr}/k_{o,par}$, was applied. The calculated reaction parameters are presented in Table 6.

For the calculations of the pre-exponential factors (k_o) and the apparent activation energies (E_{app}), data for conversions below 30% were used. Under such reaction conditions, the calculated values for the average effectiveness factors (accounting for the irregular-shaped catalyst particles) were within the limits 0.90–0.99, and therefore, the effect of the internal diffusion effect was implemented in the reactor model by applying an iterative approach. The external mass transfer limitations were minimized by tests at high hourly space velocities. Obviously, in all cases, the treatment of the samples led to an increase in activity. Within the propane combustion, the improvement in activity was within the limits of 5% to 56%, i.e., the calculated values of $k_{o,tr}/k_{o,par}$ were 1.05 for Si/Al = 23 and 1.56 for Si/Al = 50. More remarkable is the effect of the treatment for the n-hexane combustion, and again, the highest value of $k_{o,tr}/k_{o,par}$ was obtained after the treatment of the Si/Al = 50 sample. It should be pointed out that improvement of more than twofold in the activity of the Si/Al = 40 sample after the treatment is also significant. The most impressive increase is the case of the treated Si/Al = 50 sample during *n*-hexane combustion, where the reaction rate increased by more than six times.

Table 6. Calculated reaction parameters of parent and treated Co-ZSM-5 catalysts with different Si/Al ratios (23, 40 and 50).

	Propane			***n*-hexane**		
	Si/Al = 23 par	**Si/Al = 40 par**	**Si/Al = 50 par**	**Si/Al = 23 par**	**Si/Al = 40 par**	**Si/Al = 50 par**
k_o, s^{-1}	1.24×10^5	1.11×10^6	2.74×10^5	3.56×10^8	9.53×10^8	2.04×10^8
E_{app}, kJ/mol	81.89	92.11	91.87	117.68	123.43	125.85
	Si/Al = 23 tr	**Si/Al = 40 tr**	**Si/Al = 50 tr**	**Si/Al = 23 tr**	**Si/Al = 40 tr**	**Si/Al = 50 tr**
k_o, s^{-1}	5.17×10^4	2.49×10^5	1.23×10^6	8.96×10^6	3.30×10^7	1.42×10^8
E_{app}, kJ/mol	75.0	85.1	97.3	99.7	104.0	114.9
$E_{app,\,average}$, kJ/mol	80.2	88.6	94.6	108.7	113.7	120.4
$k_{o,tr}/k_{o,par}$	1.16	1.05	1.56	1.09	2.08	6.19

3. Materials and Methods

3.1. Catalyst Preparation

The starting ZSM-5 materials with different Si/Al ratios were kindly provided by SUD-CHEMIE AG (H-MFI-90, Si/Al = 50) and ALSIPENTA zeolite GmbH (SH-27, Si/Al = 23), respectively. The ZSM-5 sample of Si/Al = 40 ratio was synthesized according to [46]. All these samples were denoted as (ZSM-5-par).

The treated ZSM-5 samples (ZSM-5-tr) were modified via etching using an aqueous solution of hydrofluoric acid (Sigma-Aldrich, Taufkirchen, Germany) and ammonium fluoride (Sigma-Aldrich, Taufkirchen, Germany). The solution was prepared from 60 mL 0.25 mol/L HF acid, 10 g NH_4F and 60 g H_2O, to which 1 g of well-dispersed ZSM-5 was added. The so-obtained mixture was stirred for 20 min at 25 °C and then followed by filtration, washing and drying at 80 °C.

The precursors were prepared by the introduction of ZSM-5-tr to an aqueous solution of $Co(C_2H_3O_2)_2.4H_2O$ to obtain a 5 wt.% Co-ZSM-5-tr catalyst. The support was kept in the solution for 5 min, after which the solution was separated and the sample was dried at 100 °C. After drying, the sample was placed again in the rest of the solution. The procedure was repeated until the solution was completely absorbed. Finally, all samples were calcined for 3 h at 450 °C in the air flow.

Taking into account the dissolved amount of $Co(C_2H_3O_2)_2.4H_2O$, the final concentration of cobalt in the as-prepared samples was 5%.

3.2. Catalyst Characterization

The crystalline structure and phase composition of the samples were investigated via an Empyrean diffractometer (PANalytical) equipped with a multichannel detector (Pixel 3D, PANalytical) using Cu Kα 45 kV–40 mA radiation in the 2θ range. The quantitative phase compositions of the samples were obtained by using the X'Pert HighScore software.

The elemental analysis was carried out through WDXRF (Wave-dispersive X-ray fluorescence) using a Spectrometer Rigaku Supermini 200.

The texture characteristics of the studied catalyst samples were determined through low-temperature (77.4 K) nitrogen adsorption on a Quantachrome Instruments NOVA 1200e (Boynton Beach, FL, USA) instrument. The specific surface areas were calculated using the Brunauer–Emmett–Teller (BET) equation. The total pore volumes and average pore diameters were estimated at a relative pressure close to 0.99. The t-plot method was used to determine the volume of micropores [47]. Before the measurements, the samples were degassed for 16 h in vacuum at 200 °C. The scanning electron microscopy (SEM) analyses were performed on a Philips 515 instrument at a 20 kV accelerating voltage.

X-ray photoelectron measurements were performed on an ESCALAB MkII (VG Scientific, now Thermo Scientific, Waltham, MA, USA) electron spectrometer with a base pressure in the analysis chamber of 5×10^{-10} mbar (9×10^{-8} mbar during measurement),

equipped with a twin anode MgKα/AlKα non-monochromated X-ray source using excitation energies of 1253.6 eV and 1486.6 eV, respectively. The measurements were performed using only an AlKα non-monochromated X-ray source (1486.6 eV). The pass energy of the hemispherical analyzer was 20 eV. The instrumental resolution was measured as the full width at a half maximum (FWHM) of the Ag3d5/2, photoelectron peak is about 1 eV. The energy scale calibration was performed by normalizing the Si2p line to 103.3 eV for electrostatic sample charging. The obtained data were analyzed using SpecsLab2 Casa XPS 2.3.25 software (Casa Software Ltd., Berlin, Germany). The processing of the spectra involved a subtraction of the X-ray satellites using a Shirley-type background [48]. The peak positions and areas were determined through a symmetrical Gaussian–Lorentzian curve fitting. The relative concentrations of the different chemical species were evaluated based on the normalization of the peak areas to their photoionization cross-sections, as calculated by Scofield [49].

The temperature-programmed reduction via hydrogen (H_2/TPR) was carried out using a 10 mL.min^{-1} flow of 10% H_2 in argon and a temperature ramp of 10 °C min^{-1} up to 700 °C. Prior to the TPR experiments, the samples were treated in argon flow at 150 °C for 1 h.

The ultraviolet–visible (UV-vis) spectra were recorded on a Thermo Scientific Evolution 300 spectrophotometer, equipped with a Praying Mantis Diffuse Reflectance Accessory (Thermo Fisher Scientific).

NMR spectra were recorded on a Bruker Avance II+ 600 NMR spectrometer operating at a 599.98 MHz 1H frequency (119.20 MHz for ^{29}Si, 156.34 MHz for ^{27}Al), using a 4 mm solid-state CP/MAS dual 1H/X probe head. The samples were loaded into 4 mm zirconia rotors and spun at magic-angle spinning (MAS) rates of 10 kHz for ^{29}Si spectra and 14 kHz for ^{27}Al spectra. The quantitative ^{29}Si NMR spectra were recorded via a single-pulse sequence, 90° pulse length of 4.5 µs, 3 K time domain data points, spectrum width of 29 kHz, 1024 scans and a relaxation delay of 120 s. The spectra were processed using an exponential window function (line broadening factor 50) and were zero-filled to 16 K data points. The ^{27}Al spectra were recorded using a single-pulse sequence, 90° pulse length of 2.8 µs, 128 K time domain data points, spectrum width of 780 kHz, 1024 scans and a relaxation delay of 0.5 s. The spectra were processed via an exponential window function (line-broadening factor 50). The ^{1}H→^{29}Si cross-polarization MAS (CP-MAS) spectra were acquired with the following experimental parameters: ^{1}H excitation pulse of 3.6 µs, 2 ms contact time, 5 s relaxation delay, more than 20,000 scans and a MAS rate of 10 kHz. A ^{1}H SPINAL-64 decoupling scheme was used during CP acquisition experiments.

3.3. Catalytic Activity

The tests of the complete catalytic oxidation reactions of propane and *n*-hexane on the Co-ZSM-5 catalyst samples were carried out in a fixed bed reactor with a gaseous hourly space velocity ($GHSV_{STP}$) of 100.000 h^{-1}. The reaction temperature was controlled in such a way that the maximal deviation did not exceed +/−1 °C. The inlet concentrations of propane and *n*-hexane feed were 0.03 or 0.035 vol. %, respectively, and the oxygen was at −16.0 vol. %. All the feed gas mixtures were balanced to 100% with nitrogen (4.6). The total catalyst bed volume was adjusted to 0.5 cm^3 (0.3 cm^3 catalyst and 0.2 cm^3 quartz—glass particles) and the reactor diameter was 6.0 mm (Dreactor/Dparticles ≥ 10). Online gas-analyzers ($CO/CO_2/O_2$, Teledyne, Model T803, Teledyne API, Carroll Canyon Road, San Diego, CA 92131, USA, 2011) and THC-FID (Horiba, Kyoto, Japan) were used for the analysis of the total hydrocarbon content.

4. Conclusions

The modification of zeolites ZSM-5 with a different Si/Al ratio with a buffer solution of HF and NH_4F led to obtaining a material with secondary mesoporosity. The deposition of cobalt from an aqueous solution of $Co(C_2H_3O_2)_2.4H_2O$ on the surface of treated samples generated the formation of different cobalt oxide species: bulk-like Co_3O_4 phases strongly

interacted with the support, the Co^{2+} in ion-exchange positions (γ and β sites) and silicate-like phases. The mechanism of cobalt silicate phase formation was proposed, and it included a replacement of silanol groups, the bridging hydrogens by Co and the inclusion of the Co atoms in tetrahedral framework positions.

The catalysts, obtained through the use of ZSM-5 zeolites treated with HF and NH_4F, demonstrated higher activity in the reactions of propane and *n*-hexane complete oxidation compared with the catalyst samples containing untreated zeolite. Both the finer dispersion of metal particles on the hierarchical sample and the presence of secondary mesoporosity played a positive role in increasing catalytic activity. The creation of additional porosity improved the access of the reagents to the active sites.

Author Contributions: S.T. and A.N.: results analysis, writing—original draft preparation, conceptualization and discussion; A.N., R.V. and G.I.: catalytic test, experiments and analysis; P.S. preformed and discussed NMR analysis, H.K. performed and discussed XPS analysis; I.Y. BET measurements; B.G.: sample synthesis; K.T.: TPR measurements; S.T., A.N. and R.V.: supervision and project administration. All authors contributed to the discussion of the manuscript. All authors have read and agreed to the published version of the manuscript.

Funding: The authors express their gratitude to the National Science Fund of Bulgaria for financial support under the Contract KP-06-H49/4.

Data Availability Statement: The data presented in this study are available on request from the corresponding author.

Acknowledgments: Research equipment of Distributed Research Infrastructure INFRAMAT, part of the Bulgarian National Roadmap for Research Infrastructure, supported by the Bulgarian Ministry of Education and Science, was used in this investigation.

Conflicts of Interest: The authors declare no conflict of interest.

References

1. Spivey, J.J. Complete catalytic oxidation of volatile organics. *Ind. Eng. Chem. Res.* **1987**, *26*, 2165–2180. [CrossRef]
2. Baldi, M.; Finocchio, E.; Milella, F.; Busca, G. Catalytic combustion of C3 hydrocarbons and oxygenates over Mn_3O_4. *Appl. Catal. B Environ.* **1998**, *16*, 43–51. [CrossRef]
3. Larsson, P.-O.; Andersson, A.; Wallenberg, L.R.; Svenssonb, B. Combustion of CO and Toluene; Characterisation of Copper Oxide Supported on Titania and Activity Comparisons with Supported Cobalt, Iron, and Manganese Oxide. *J. Catal.* **1996**, *163*, 279–293. [CrossRef]
4. Niaei, A.; Salari, D.; Hosseini, S.A.; Khatamian, M.; Jodael, A. Catalytic Combustion of Ethyl Acetate over Nanostructure Cobalt Supported ZSM-5 Zeolite Catalysts. *Chin. J. Chem.* **2009**, *27*, 483–488. [CrossRef]
5. Scirè, S.; Minicò, S.; Crisafulli, C. Selective hydrogenation of phenol to cyclohexanone over supported Pd and Pd-Ca catalysts: An investigation on the influence of different supports and Pd precursors. *Appl. Catal. B Environ.* **2003**, *45*, 117–125. [CrossRef]
6. International Zeolite Association. Database of Zeolite Structures—MFI. Available online: http://europe.iza-structure.org/IZA-SC/framework.php?STC=MFI (accessed on 1 March 2023).
7. Díaz, I.; Kokkoli, E.; Terasaki, O.; Tsapatsis, M. Surface Structure of Zeolite (MFI) Crystals. *Chem. Mater.* **2004**, *16*, 5226–5232. [CrossRef]
8. Kokotailo, G.; Lawton, S.; Olson, D.; Meier, W.M. Structure of synthetic zeolite ZSM-5. *Nature* **1978**, *272*, 437–438. [CrossRef]
9. Sato, H.; Ishii, N.; Hirose, K.; Nakamura, S. New developments in zeolite science and technology. In *Studies in Surface Science and Catalysis*; Murak, A.I.Y., Ward, J.W., Eds.; Elsevier: Amsterdam, The Netherlands, 1986; Volume 28, pp. 755–762. [CrossRef]
10. Zhou, Q.; Wang, Y.-Z.; Tang, C.; Zhang, Y.-H. Modifications of ZSM-5 zeolites and their applications in catalytic degradation of LDPE. *Polym. Degrad. Stab.* **2003**, *80*, 23–30. [CrossRef]
11. Groen, J.C.; Zhu, W.; Brouwer, S.; Huynink, S.J.; Kapteijn, F.; Moulijn, J.A.; Pérez-Ramírez, J. Direct Demonstration of Enhanced Diffusion in Mesoporous ZSM-5 Zeolite Obtained via Controlled Desilication. *J. Am. Chem. Soc.* **2007**, *129*, 355–360. [CrossRef]
12. Hartmann, M.; Machoke, A.G.; Schwieger, W. Catalytic test reactions for the evaluation of hierarchical zeolites. *Chem. Soc. Rev.* **2016**, *45*, 3313–3330. [CrossRef] [PubMed]
13. Qin, Z.; Gilson, J.-P.; Valtchev, V. Mesoporous zeolites by fluoride etching. *Curr. Opin. Chem. Eng.* **2015**, *8*, 1–6. [CrossRef]
14. Kalvachev, Y.; Todorova, T.; Popov, C. Recent Progress in Synthesis and Application of Nanosized and Hierarchical Mordenite—A Short Review. *Catalysts* **2021**, *11*, 308. [CrossRef]
15. Velinova, R.; Grahovski, B.; Kolev, H.; Ivanov, G.; Todorova, S.; Naydenov, A. Reaction kinetics and mechanism of the catalytic oxidation of propane over Co–ZSM-5 zeolites. *React. Kinet. Mech. Catal.* **2022**, *135*, 83–103. [CrossRef]

16. Velinova, R.; Grahovski, B.; Kolev, H.; Ivanov, G.; Todorova, S.; Naydenov, A. Reaction kinetics and mechanism of n-hexane catalytic combustion over Co-ZSM-5 zeolites. *Mater. Today Proc.* **2022**, *61*, 1255–1259. [CrossRef]
17. Todorova, T.; Petrova, P.; Kalvachev, Y. Catalytic Oxidation of CO and Benzene over Metal Nanoparticles Loaded on Hierarchical MFI Zeolite. *Molecules* **2021**, *26*, 5893. [CrossRef]
18. Kalvachev, Y.; Todorova, T.; Nihtianova, D.; Lazarova, H.; Popova, M. Fluoride etching of mordenite and its influence on catalytic activity. *J. Mater. Sci.* **2017**, *52*, 5297–5308. [CrossRef]
19. Treacy, M.M.J.; Higgins, J.B. *Collection of simulated XRD powder patterns for zeolites*, 4th ed.; Elsevier: Amsterdam, The Netherlands, 2001.
20. Allen, G.C.; Hallam, K.R. Characterisation of the spinels MxCo1−xFe2O4 (M = Mn, Fe or Ni) using X-ray photoelectron spectroscopy. *Appl. Surf. Sci.* **1996**, *93*, 25–30. [CrossRef]
21. Gautier, J.L.; Rios, E.; Gracia, M.; Marco, J.F.; Gancedo, J.R. Characterisation by X-ray photoelectron spectroscopy of thin MnxCo3−xO4(1≥x≥0) spinel films prepared by low-temperature spray pyrolysis. *Thin Solid Film.* **1997**, *311*, 51–57. [CrossRef]
22. Shanke, D.; Vada, S.; Blekkan, E.A.; Hilmen, E.A.; Hoff, A.; Holmen, A. Study of Pt-Promoted Cobalt CO Hydrogenation Catalysts. *J. Catal.* **1995**, *156*, 85–95. [CrossRef]
23. Todorova, S.; Blin, J.L.; Naydenov, A.; Lebeau, B.; Kolev, H.; Gaudin, P.; Dotzeva, A.; Velinova, R.; Filkova, D.; Ivanova, I.; et al. Co3O4-MnOx oxides supported on SBA-15 for CO and VOCs oxidation. *Catal. Today* **2019**, *357*, 602–612. [CrossRef]
24. Todorova, S.; Naydenov, A.; Kolev, H.; Tenchev, K.; Ivanov, G.; Kadinov, G. Effect of Co and Ce on silica supported manganese catalysts in the reactions of complete oxidation of n-hexane and ethyl acetate. *J. Mater. Sci.* **2011**, *46*, 7152–7159. [CrossRef]
25. Khodakov, A.Y.; Bechara, R.; Griboval-Constant, A. Fischer–Tropsch synthesis over silica supported cobalt catalysts: Mesoporous structure versus cobalt surface density. *Appl. Catal. A Gen.* **2003**, *254*, 273–288. [CrossRef]
26. Khodakov, A.; Lynch, J.; Bazin, D.; Rebours, B.; Zanier, N.; Moisson, B.; Chaumette, P. Reducibility of Cobalt Species in Silica-Supported Fischer–Tropsch Catalysts. *J. Catal.* **1997**, *168*, 16–25. [CrossRef]
27. Lónyi, F.; Solt, H.E.; Pászti, Z.; Valyon, J. Mechanism of NO-SCR by methane over Co,H-ZSM-5 and Co,H-mordenite catalysts. *Appl. Catal. B Environ.* **2014**, *150–151*, 218–229. [CrossRef]
28. Shilina, M.I.; Rostovshchikova, T.N.; Nikolaev, S.A.; Udalova, O.V. Polynuclear Co-oxo cations in the catalytic oxidation of CO on Co-modified ZSM-5 zeolites. *Mater. Chem. Phys.* **2019**, *223*, 287–298. [CrossRef]
29. Wang, X.; Chen, H.; Sachtler, W.M.H. Catalytic reduction of NOx by hydrocarbons over Co/ZSM-5 catalysts prepared with different methods. *Appl. Catal. B Environ.* **2000**, *26*, L227–L239. [CrossRef]
30. Wang, X.; Chen, H.; Sachtler, W.M.H. Selective reduction of NOx with hydrocarbons over Co/MFI prepared by sublimation of CoBr2 and other methods. *Appl. Catal. B Environ.* **2001**, *29*, 47–60. [CrossRef]
31. Mhamdi, M.; Khaddar-Zine, S.; Ghorbel, A. Influence of the method of ion exchange and cobalt loading on the physico-chemical and catalytic properties of Co-ZSM-5 catalysts. *React. Kinet. Catal. Lett.* **2006**, *88*, 149–156. [CrossRef]
32. Dedecek, J.; Kaucky, D.; Wichterlova, B. Co2+ ion siting in pentasil-containing zeolites, part 3.: Co2+ ion sites and their occupation in ZSM-5: A VIS diffuse reflectance spectroscopy study. *Microporous Mesoporous Mater.* **2000**, *35–36*, 483–494. [CrossRef]
33. Chupin, C.; van Veen, A.C.; Konduru, M.; Després, J.; Mirodatos, C. Identity and location of active species for NO reduction by CH4 over Co-ZSM-5. *J. Catal.* **2006**, *241*, 103–114. [CrossRef]
34. Fierro, G.; Eberhardt, M.A.; Houalla, M.; Hercules, D.M.; Keith Hall, W. Redox Chemistry of CoZSM-5 Zeolite. *J. Phys. Chem.* **1996**, *100*, 8468–8477. [CrossRef]
35. Szegedi, Á.; Popova, M. Toluene hydrogenation over nickel-containing MCM-41 and Ti-MCM-41 materials. *J. Porous Mater.* **2010**, *17*, 663–668. [CrossRef]
36. Engelhardt, G.; Lohse, U.; Lippmaa, E.; Tarmak, M.; Mägi, M.Z. 29Si-NMR-Untersuchungen zur Verteilung der Silicium-und Aluminiumatome im Alumosilicatgitter von Zeolithen mit Faujasit-Struktur. *Anorg. Allg. Chem.* **1981**, *11*, 49–64. [CrossRef]
37. Massiot, D.; Fayon, F.; Capron, M.; King, I.; Le Calve, S.; Alonso, B.; Durand, J.O.; Bujoli, B.; Gan, Z.; Hoatson, G. Modelling one- and two-dimensional solid-state NMR spectra. *Magn. Reson. Chem.* **2002**, *40*, 70–76. [CrossRef]
38. Hunger, M. Solid-State NMR Spectroscopy, Chapter 2. In *Zeolite Characterization and Catalysis*; Chester, A.W., Derouane, E.G., Eds.; Springer: Berlin/Heidelberg, Germany, 2009; pp. 65–105.
39. Brunner, E.; Ernst, H.; Freude, D.; Froehlich, T.; Hunger, M.; Pfeifer, H. Magic-angle-spinning NMR studies of acid sites in zeolite H-ZSM-5. *J. Catal.* **1991**, *127*, 34–41. [CrossRef]
40. Popova, M.; Szegedi, Á.; Oykova, M.; Lazarova, H.; Koseva, N.; Mihályi, M.R.; Shestakova, P. Selective Production of Phenol on Bifunctional, Hierarchical ZSM-5 Zeolites. *Molecules* **2021**, *26*, 3576. [CrossRef]
41. Todorova, T.; Shestakova, P.; Petrova, T.; Popova, M.; Lazarova, H.; Kalvachev, Y. Fluoride etching of AlZSM-5 and GaZSM-5 zeolites. *J. Mater. Sci.* **2020**, *55*, 13799–13814. [CrossRef]
42. Mhamdi, M.; Marceau, E.; Khaddar-Zine, S.; Ghorbel, A.; Che, M.; Ben Taarit, Y.B.; Villain, F. Formation of Cobalt Phyllosilicate During Solid State Preparation of Co2+/ZSM5 Catalysts from Cobalt Acetate. *Catal. Lett.* **2004**, *98*, 135–140. [CrossRef]
43. Huang, J.; Jiang, Y.; Reddy Marthala, V.R.; Thomas, B.; Romanova, E.; Hunger, M. Characterization and Acidic Properties of Aluminum-Exchanged Zeolites X and Y. *J. Phys. Chem. C* **2008**, *112*, 3811–3818. [CrossRef]
44. van Bokhoven, J.A.; Roest, A.L.; Koningsberger, D.C.; Miller, J.T.; Nachtegaal, G.H.; Kentgens, A.P.M. Changes in Structural and Electronic Properties of the Zeolite Framework Induced by Extraframework Al and La in H-USY and La(*x*)NaY: A^{29}Si and^{27}Al MAS NMR and^{27}Al MQ MAS NMR Study. *J. Phys. Chem. B* **2000**, *104*, 6743–6754. [CrossRef]

45. Lim Suh, B.; Kim, J. Reverse shape selectivity of hexane isomer in ligand inserted MOF-74. *RSC Adv.* **2020**, *10*, 22601–22605. [CrossRef]
46. Hardenberg, T.; Mertens, L.; Mesman, P.; Muller, H.; Nicolaides, C. A catalytic method for the quantitative evaluation of crystallinites of ZSM-5 zeolite preparations. *Zeolites* **1992**, *12*, 685–689. [CrossRef]
47. Galarneau, A.; Villemot, F.; Rodriguez, J.; Fajula, F.; Coasne, B. Validity of the *t-plot* Method to Assess Microporosity in Hierarchical Micro/Mesoporous Materials. *Langmuir* **2014**, *30*, 13266–13274. [CrossRef] [PubMed]
48. Shirley, D. High-Resolution X-Ray Photoemission Spectrum of the Valence Bands of Gold. *Phys. Rev. B* **1972**, *5*, 4709–4714. [CrossRef]
49. Scofield, J.H. Hartree-Slater subshell photoionization cross-sections at 1254 and 1487 eV. *J. Electron Spectrosc. Relat. Phenom.* **1976**, *8*, 129–137. [CrossRef]